The Journal of Chemical Physics

HD ($v = 1, j = 2, m$) orientation controls HD–He rotationally inelastic scattering near 1 K

Cite as: J. Chem. Phys. **150**, 174301 (2019); https://doi.org/10.1063/1.5096531
Submitted: 18 March 2019 . Accepted: 09 April 2019 . Published Online: 02 May 2019

William E. Perreault, Nandini Mukherjee, and Richard N. Zare

The Journal of Chemical Physics ARTICLE scitation.org/journal/jcp

HD (v = 1, j = 2, m) orientation controls HD–He rotationally inelastic scattering near 1 K

Cite as: J. Chem. Phys. 150, 174301 (2019); doi: 10.1063/1.5096531
Submitted: 18 March 2019 • Accepted: 9 April 2019 •
Published Online: 2 May 2019

William E. Perreault, Nandini Mukherjee,[a] and Richard N. Zare[a]

AFFILIATIONS

Department of Chemistry, Stanford University, Stanford, California 94305, USA

[a]Authors to whom correspondence should be addressed: nmukherj@stanford.edu and zare@stanford.edu

ABSTRACT

To investigate how molecular orientations affect low energy scattering, we have studied the rotational relaxation of HD (v = 1, j = 2, m) → (v' = 1, j' = 0) by collision with ground-state He, where v, j, and m designate the vibrational, rotational, and magnetic quantum numbers, respectively. We experimentally probed different collision geometries by preparing three specific m sublevels, including an m entangled sublevel, belonging to a single rovibrational (v = 1, j = 2) energy level within the ground electronic state of HD using Stark-induced adiabatic Raman passage. Low collision energies (0–5 K) were achieved by coexpanding a 1:19 HD:He mixture in a highly collimated supersonic beam, which has defined the direction of the collision velocity and restricted the incoming orbital angular momentum states, defined by the quantum number l, to $l \leq 2$. Partial wave analysis of experimental data shows that a single $l = 2$ input orbital dominates the scattered angular distribution, implying the presence of a collisional resonance. The differential scattering angular distribution exhibits a greater than fourfold stereodynamic preference for the $m = 0$ input state vs $m = \pm 2$, when the quantization axis is oriented parallel to the collision velocity.

INTRODUCTION

Molecular scattering experiments interrogate the forces that govern interactions at the quantum level,[1,2] but the amount of detailed information that can be extracted from a scattering experiment is limited by how precisely the input and output quantum states are defined.[3,4] In particular, because of the anisotropic nature of molecular forces, the result of a scattering experiment strongly depends on the collision geometry, which is defined by the orientation of the molecular axis relative to the collision velocity. At low collision energies, even low barriers in the potential energy landscape become dominant factors in a scattering process. These scattering events are thus particularly sensitive to weak anisotropic forces and therefore depend sensitively on the molecular orientation. Moreover, the significant obstacle posed by even a weak barrier means that van der Waals resonances become increasingly important as the collision energy decreases. Combined, these two sensitivities make it possible to observe the effect of molecular orientation on the formation of collisional resonances.

To investigate the importance of molecular orientation in low energy collisions, we have studied the rotational relaxation of HD from (v = 1, j = 2, m) to (v' = 1, j' = 0) by low energy collision (~0.1 meV) with a ground-state He atom. Here, v is the vibrational quantum number, j is the rotational quantum number, and m is the projection of the rotational angular momentum on a suitable quantization axis and defines the molecular orientation. Our ability to prepare molecules in a single rovibrational energy state with m state precision and state-selectively measure the angular distribution of rotationally relaxed HD (v = 1, j = 0) allows us to observe the effect of anisotropic forces that give rise to $\Delta j = 2$ rotational relaxation in a cold atom-diatom collision. In the special case considered here, we were able to extract much dynamical information by correlating the well-defined input quantum states with the measured outgoing states using partial wave analysis, revealing the fingerprint of a collisional resonance. Using quantum state selected scattering of NO with He, Vogels *et al.* previously demonstrated that in the presence of collisional resonance the resonant partial wave dominates the scattering angular distribution.[5] The nearly complete control achieved in the present study is in contrast with our earlier work on the rotationally inelastic collisions of HD with H_2 and D_2 molecules,[6,7] where the partner molecule was not state-selected and so the input channel remained only partially defined.

Preparing a large molecular ensemble in a coherently defined input state with sufficient density to measure inelastic scattering poses a considerable experimental challenge.[4,8] A variety of techniques have been developed to prepare or control both the internal[9–12] and external[13,14] quantum states. In this work, the internal quantum state of HD ($v = 1, j = 2, m$) was prepared using a coherent optical technique, known as Stark-induced adiabatic Raman passage (SARP).[15] Using a pair of partially overlapping nanosecond pulses, SARP transfers nearly the entire population of the ($v = 0, j = 0$) ground state to the desired rovibrationally excited target state and simultaneously prepares the molecules in a single or superposition of specific m states.[16–18] Control over the external or orbital state of the colliding partners was achieved by coexpanding the two gases in the same molecular beam, which defined both the magnitude and direction of the collision velocity in the lab frame.[19,20] This technique ensured that only a few orbital states contributed to the collision by substantially reducing the HD–He relative speed (collision temperature).

We studied the scattering of HD molecules prepared in three specific m state orientations, including an m entangled state, within the ($v = 1, j = 2$) energy eigenstate to elucidate the stereodynamics of the scattering process. The selection of the m state defines the orientation of the molecular bond axis relative to the collision velocity in the center of mass frame. The partial wave analysis of our experimental data showed a striking fourfold preference for the $m = 0$ input state in the $\Delta j = 2$ rotational relaxation of HD. With few partial waves involved in the low temperature collision, it was possible to show a clear dominance of a single $l = 2$ input orbital wave, suggesting a scattering resonance that is sensitive to molecular orientation.

Historically, the rotationally inelastic scattering of hydrogenic as well as many other systems has been studied extensively.[21–23] Additionally, many studies have been conducted on rotationally inelastic collisions of NO with rare gas atoms that examined the angular momentum polarization of collision products as a function of the scattering angle,[24–26] but none of these studied the effects of input collision geometry. To our knowledge, this salient question for experimental quantum mechanics has only been addressed in a few prior studies on OH[27] and NO[28,29] collisions with rare gas atoms at a high temperature. Presented here are the first measurements that probe the effect of collision geometry on low energy inelastic scattering. Furthermore, this experimental study is the first on low-temperature hydrogen-helium scattering, which is of astrophysical importance[30–32] and is also immensely valuable as a test bed for quantum mechanical scattering calculations.[32–35]

EXPERIMENTAL METHODS

A molecular beam is formed when a mixture of 5% HD (98%, Cambridge Isotope Labs) in He (99.995%, Praxair) is coexpanded into a high vacuum source chamber using a room-temperature Even-Lavie pulsed valve[36] operated at a stagnation pressure of 14 bars (~200 psi). To reduce the transverse velocity spread of the HD and He, we collimate the beam using a skimmer of diameter 600 μm, kept at a distance of ~8 cm from the pulsed valve. The skimmer opening is located ~3.5 cm upstream of the interaction region. Using (2 + 1) REMPI with UV pulses (5 ns, 201.4 nm) to detect HD ($v = 0, j = 0$), we measure the diameter of the molecular beam in the interaction region to be ~1.5 mm. This information allows us to determine the transverse beam divergence to be ~12 mrad, corresponding to a maximum transverse velocity of ~26 m/s. The coexpansion thus defines the relative velocity direction of the colliding partners, considerably simplifying the analysis of the scattering angular distribution. REMPI measurements of the rotational distribution of the supersonically cooled HD in the molecular beam showed that greater than 98% of the population is cooled to the HD ($v = 0, j = 0$) ground state. All REMPI pulses are obtained by using two different β-barium borate crystals in sequence to generate the third harmonic of a tunable pulsed dye laser (ND6000, Continuum Lasers, Inc.) pumped by a Q-switched Nd^{3+}:YAG laser (PL9020, Continuum Lasers, Inc.).

The longitudinal velocities of both HD and He were characterized by measuring the time-of-flight spectrum following REMPI ionization. He atoms were ionized using (4 + 1) REMPI with UV pulses (5 ns, 240.6 nm) through the intermediate 1s2s state (see the supplementary material). The measured velocity distributions of both the HD and He ions are artificially increased compared to the velocity distribution of the neutral molecule or atom by the recoil of the REMPI photoelectron. The neutral velocity distributions were extracted by deconvoluting the effects of the recoil from the measured time-of-flight spectra.[19,37] By convoluting the measured velocity distributions of each neutral species, we determined the relative velocity distribution shown in Fig. 1(a). From this, we calculated the collision energy distribution shown in Fig. 1(b), which showed that 90% of scattering events take place at collision energies below 5 K.

The external input state of a collision with definite linear momentum p is represented by a plane wave composed of a coherent superposition of an infinite number of orbital states. These states, known as partial waves, are characterized by the angular momentum quantum number l and are correlated to a classical impact parameter $b = \hbar\sqrt{l(l+1)}/(\mu u_r)$, where μ is the reduced mass and u_r is the relative speed. As shown in Fig. 1, coexpanding the two gases in the same molecular beam substantially reduced the relative speed. Considering the range of collision energies shown in Fig. 1(b), we find that the HD–He interaction potential becomes negligible at a radius of ~6 Å.[33] Using 6 Å as the maximum possible value of the classical impact parameter and the relative speed distribution shown in Fig. 1(a), we can infer that the input partial waves that contribute to the scattering process are limited to $l \leq 2$. By restricting the number of involved orbital states in the input channel, we were able to correlate the output scattered states to specific input states and express the angular distribution in terms of the relevant scattering matrix elements.

To achieve nearly complete control over the input channel of our collision system, we used SARP to prepare the internal state of the HD molecules in the beam. SARP accomplishes greater than 90% population transfer using a sequence of partially overlapping single-mode pump and Stokes laser pulses. By inducing a second-order Stark shift of the rovibrational levels, the stronger pump pulse (10 ns, 532 nm, 10 J/mm^2) sweeps the Raman frequency through resonance twice during the rising and falling intensity of its temporal profile. Population is transferred adiabatically from HD ($v = 0$, $j = 0$) to HD ($v = 1, j = 2$) in the presence of the Stokes pulse (5 ns, 670 nm, 2 J/mm^2) at the second resonance crossing. This occurs so long as the frequency difference between the pump and Stokes laser

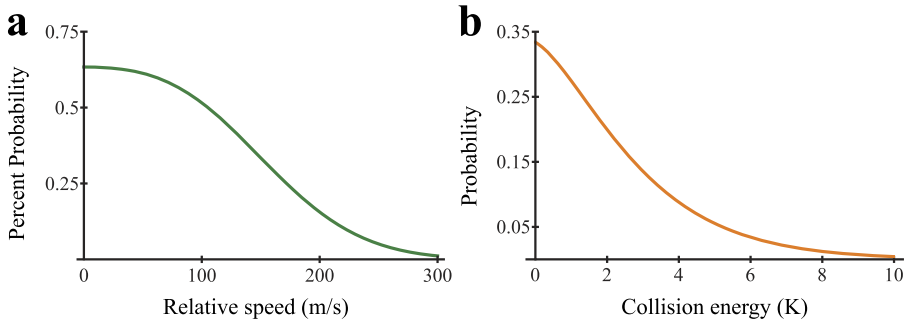

FIG. 1. Relative speed and collision energy. (a) Relative speed distribution between HD ($v = 1, j = 2$) and He in the mixed molecular beam derived by convoluting the velocity distributions of the two individual species measured in the mixed molecular beam by time-of-flight mass spectrometry. (b) Collision energy distribution for the HD/He scattering determined from the relative speed distribution shown in (a). 90% of collisions take place at collision energies between 0 and 5 K.

pulses is tuned to within a few gigahertz of the Raman resonance in HD (116.546 THz). SARP requires a threshold laser power to satisfy the adiabatic following condition, defined by $d\Delta/dt < 2\pi\Omega_R{}^2$, where Ω_R is the Rabi frequency for the HD ($v = 0, j = 0$) → ($v = 1, j = 2$) Raman transition and $d\Delta/dt$ is the Stark-induced sweeping rate of the dynamic Raman detuning Δ. More detailed descriptions of SARP can be found elsewhere.[16–18,38] The pump pulse is obtained from the second harmonic of an injection-seeded, Q-switched Nd^{3+}:YAG laser (PRO-290, Spectra-Physics), and the Stokes pulse is derived from a pulsed dye amplifier (PrecisionScan, Sirah) which is seeded by a frequency stabilized ring dye laser (Matisse, Sirah) and pumped by the same Nd^{3+}:YAG laser used to generate the pump pulse. All of our Nd^{3+}:YAG lasers operate synchronously with the pulsed valve at a repetition rate of 20 Hz. Following an optical delay of 6 ns, the Stokes laser pulse is combined with the pump pulse on a dichroic beam splitter. Both beams are then focused onto the molecular beam using a 40 cm focal length lens. Using (2 + 1) REMPI with UV pulses (209.3 nm, 5 ns) to detect the SARP-produced HD ($v = 1, j = 2$), the region of the molecular beam excited by SARP is experimentally measured to have a diameter of ~100 μm. The various m components of HD ($v = 1, j = 2$) in the H-SARP, V-SARP, and X-SARP states discussed below were generated by choosing different polarization directions of the pump and Stokes laser pulses relative to the fixed molecular beam axis. It is important to note that the lab-frame choice of laser polarization translates neatly into a center-of-mass frame molecular orientation because the collision velocity is well-defined in the lab frame as a result of the narrow divergence of the molecular beam. We were therefore able to directly interrogate the stereodynamics of the collision process.

The scattering product state HD ($v' = 1, j' = 0$) is state-selectively ionized by (2 + 1) REMPI with 209.1 nm UV pulses. The REMPI probe beam (5 ns, 209.1 nm, 0.3 J/mm^2) is focused onto the molecular beam using a 60 cm lens to a spot size of ~20 μm. The probe polarization is held perpendicular to the time-of-flight axis to minimize the effect of recoil from the REMPI photoelectron on the measured time-of-flight of the scattered product.[19,37] The REMPI generated ions are detected on a multichannel plate (MCP) at the end of a time-of-flight mass spectrometer connected to the reaction chamber. The velocity distribution of the scattered molecules along the molecular beam axis is directly determined from the measured time-of-flight spectrum. Because the scattering center-of-mass frame coincides with the moving frame of reference of the molecular beam, the scattering angular distribution can then be easily extracted from the velocity distribution using the final speed of the scattered HD molecules calculated from conservation of energy.[6,7]

HD–HE STEREODYNAMICS

In order to interrogate the stereodynamics of the HD ($v = 1, j = 2$) → ($v' = 1, j' = 0$) rotational relaxation by collision with He, it was necessary to prepare three different m states of the ($v = 1, j = 2$) level. Two of the three m states studied in this paper were prepared using parallel pump and Stokes polarizations. As described in detail in our earlier work,[6,7] the HD bond axis in these two states was preferentially polarized either parallel or perpendicular to the direction of the collision velocity (relative velocity between the HD and He). To simplify our data analysis, we have chosen the angular momentum quantization axis along this direction. When the pump and Stokes laser pulses are polarized parallel to the quantization axis, which we call H-SARP, the excited HD molecules are prepared in the state given by

$$\Psi_H = |v = 1, j = 2, m = 0\rangle \quad (1)$$

with their bond axis preferentially aligned parallel to the collision velocity (see the inset of Fig. 2). When the pump and Stokes laser pulses are polarized perpendicular to the quantization axis, which we call V-SARP, the excited HD molecules are prepared in the superposition state

$$\Psi_V = |j = 2, m' = 0\rangle = -1/2|j = 2, m = 0\rangle + \sqrt{3/8}[|j = 2, m = 2\rangle + |j = 2, m = -2\rangle], \quad (2)$$

resulting in a preferentially perpendicular orientation of the HD bond axis to the collision velocity (see the inset of Fig. 3). In Eq. (2), m' refers to the rotational angular momentum component along the quantization Z′-axis shown in the inset of Fig. 3, whereas in both Eqs. (1) and (2) m refers to the rotational

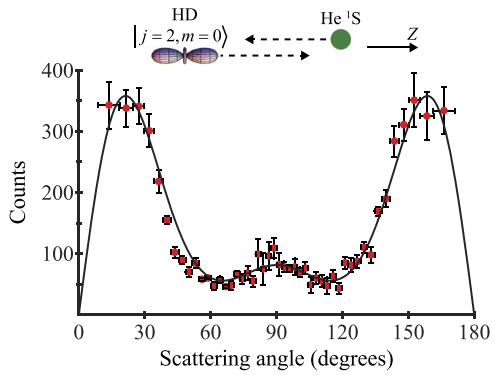

FIG. 2. HD–He H-SARP scattering angular distribution. The red dots give the experimentally measured angular distribution for scattered HD ($v' = 1$, $j' = 0$) molecules generated by rotationally inelastic collisions of HD ($v = 1$, $j = 2$, $m = 0$) with He. The experimental scattering angle is measured with respect to the +Z axis in a frame of reference moving at the center-of-mass velocity. The m quantum number gives the rotational angular momentum component along the Z-axis shown in the inset. After subtracting the off-resonant background, a total of ~8000 scattered molecules were recorded over a period of 180 000 laser pulses. The solid black curve shows the fit ($R^2 = 0.99$) to the experimental data generated as described in the text. The inset describes the input quantum state for this scattering event, wherein the HD bond axis is preferentially aligned parallel to the +Z axis.

angular momentum component along the Z-axis shown in the insets of Figs. 2 and 3. From this point forward, all angular momentum quantization will refer to the Z-axis, which is parallel to the collision velocity. As we describe in a later section, by analyzing the angular

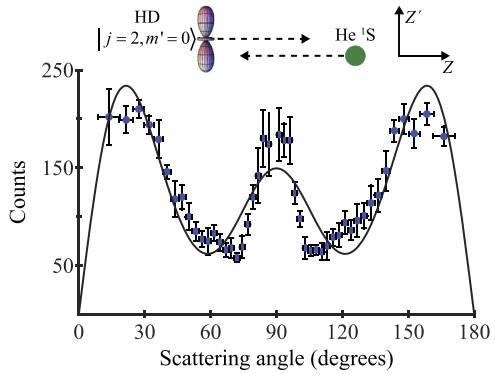

FIG. 3. HD–He V-SARP scattering angular distribution. The blue dots give the experimentally measured angular distribution for scattered HD ($v' = 1$, $j' = 0$) molecules generated by rotationally inelastic collisions of HD ($v = 1$, $j = 2$, $m' = 0$) with He. The m' quantum number gives the rotational angular momentum component along the Z′-axis shown in the inset. As shown in Eq. (2), the HD ($v = 1$ $j = 2$, $m' = 0$) state can be equivalently expressed as the superposition of HD ($v = 1$ $j = 2$, $m = 0, \pm 2$) states, where m gives the rotational angular momentum component along the Z-axis. After subtracting the off-resonant background, a total of ~7000 scattered molecules were recorded over a period of 216 000 laser pulses. The solid black curve shows the fit ($R^2 = 0.97$) to the experimental data generated as described in the text. The inset describes the input quantum state for this scattering event, wherein the HD bond axis is preferentially aligned perpendicular to the +Z axis.

distributions resulting from the scattering of the H-SARP and V-SARP states, we were able to determine the relative amplitude and phase of the various outgoing scattered states resulting from the HD $\Delta j = 2$ rotational relaxation by collision with He.

The third m state is prepared using cross-polarized pump and Stokes laser pulses, resulting in a biaxial distribution of the HD bond axis that we call X-SARP (see the inset of Fig. 4). The excitation schematic for the preparation of the X-SARP state is presented in the supplementary material. This state consists of a superposition of the $m = +1$ and $m = -1$ angular momentum components of the ($v = 1$, $j = 2$) energy eigenstate and is given by

$$\Psi_X = \sqrt{1/2}[|j=2, m=1\rangle + |j=2, m=-1\rangle]. \quad (3)$$

Ψ_X is an m entangled state, and so, unlike the V-SARP state, for any choice of the quantization axis, the X-SARP state has no $m = 0$ component. The scattering of the X-SARP state provided us with a test case against which to compare the fitted scattering amplitudes we extract from the H-SARP and V-SARP scattering.

H-SARP AND V-SARP EXPERIMENTAL RESULTS

Figures 2 and 3 show the HD–He center-of-mass angular distribution for the inelastically scattered HD ($v' = 1$, $j' = 0$) where the HD ($v = 1$, $j = 2$) bond axis is preferentially aligned parallel (H-SARP, Fig. 2) and perpendicular (V-SARP, Fig. 3) to the collision velocity, respectively. Using the procedure described in our previous publication,[6] the angular distribution was determined from the time-of-flight spectrum of the ions generated by state-selective ionization of the HD ($v' = 1$, $j' = 0$) resulting from scattering with He. We have verified that the 1:19 ratio of HD to He in our molecular beam suppresses HD–HD scattering below the noise threshold. In our experiment, the measured angular distribution is the same as the center-of-mass angular distribution (see the supplementary material), and therefore, we can extract the outgoing scattered waves' amplitude and phase directly from our data. As detailed below, we found a set of self-consistent coefficients that simultaneously optimized the fit to the measured H-SARP and V-SARP scattering angular distributions, as shown by the solid black curves in Figs. 2 and 3. The residual noise near 90°, which is generated by the off-resonant ionization of unscattered HD ($v = 1$, $j = 2$) molecules, is large in both cases. While we do subtract this off-resonant background, fluctuations and drift in the laser power make it not possible to remove completely its signature.

DETERMINATION OF OUTGOING SCATTERING STATES USING PARTIAL-WAVE ANALYSIS

The differential cross section gives the probability of scattering within a differential solid angle given by $d\Omega = \sin\theta\, d\theta\, d\varphi$, where φ gives the azimuthal angle and θ gives the polar angle with respect to the collision velocity in the center-of-mass frame, which is parallel to the quantization Z-axis defined in the inset of Fig. 2. The experimentally measured scattering angular distribution, $d\sigma/d\theta$, is related to the differential cross section, $d\sigma/d\Omega$, by integrating over the azimuthal angle φ,

$$\frac{d\sigma}{d\theta} = \sin\theta \int_0^{2\pi} \frac{d\sigma}{d\Omega} d\varphi, \quad (4)$$

because our detection scheme is not sensitive to this angle. For the H-SARP prepared HD state, Ψ_H [see Eq. (1)], the angular distribution of scattered HD ($v' = 1, j' = 0$) is given by

$$\left(\frac{d\sigma}{d\theta}\right)_H = \sin\theta \int_0^{2\pi} \left|q_{j=2,m=0\to j'=0}\right|^2 d\varphi, \tag{5}$$

where $q_{j=2,m=0\to j'=0}$ represents the amplitude for the ($v = 1$, $j = 2$, $m = 0$) → ($v' = 1$, $j' = 0$) inelastic scattering of HD into a differential solid angle $d\Omega$ in the direction (θ, φ) with respect to the quantization Z-axis. The angular distribution for the V-SARP prepared HD state, Ψ_V [see Eq. (2)], is generated by the superposition of the scattered amplitudes arising from each component m state present in Eq. (2),

$$\left(\frac{d\sigma}{d\theta}\right)_V = \sin\theta \int_0^{2\pi} \left| -\frac{1}{2} q_{j=2,m=0\to j'=0} + \sqrt{\frac{3}{8}}\left[q_{j=2,m=2\to j'=0} + q_{j=2,m=-2\to j'=0}\right]\right|^2 d\varphi. \tag{6}$$

Each of the angle-dependent scattering amplitudes q can be expanded in terms of outgoing orbital states represented by the spherical harmonics, $Y_{l',m_{l'}}(\theta,\varphi)$, as follows:

$$q_{j=2,m\to j'=0} = \sum_{l',m_{l'}} c_{l',m_{l'}} Y_{l',m_{l'}}(\theta,\varphi), \tag{7}$$

where l' represents the orbital angular momentum, $m_{l'}$ gives its component along the quantization Z axis, and $c_{l'm_{l'}}$ are the complex-valued amplitudes for each outgoing wave. The possible values of the outgoing orbital angular momentum (l', $m_{l'}$) are determined from the conservation of the total angular momentum J as well as its component M along the quantization Z-axis. As determined from the partial wave analysis discussed in the supplementary material, the possible values of l' in Eq. (7) are limited to 0, 1, 2, 3, and 4 for the collision energies present in our experiment. Because of our choice of quantization axis parallel to the collision velocity, $m_{l'}$ must be equal to m for the rotationally inelastic ($v = 1, j = 2, m$) → ($v' = 1$, $j' = 0$) collision.

Each outgoing partial wave in Eq. (7) results from the interference of the input orbital states which are scattered (diffracted) by the interaction potential, and so, the complex coefficients $c_{l'm_{l'}}$ that appear in Eq. (7) are not independent of one another. The scattering matrix, which is mathematically defined by $\Psi_{outgoing} = S\Psi_{incoming}$,[39–41] gives the transition probabilities connecting specific input and output asymptotic states. Thus, the amplitudes of the various outgoing asymptotic states $c_{l'm_{l'}}$ are interrelated by the relevant scattering matrix elements $S^J(jl; j'l')$, which represent the amplitude of an outgoing orbital l' originating from a given incoming orbital l as a result of the $j \to j'$ inelastic collision with total angular momentum J.

We have used the expression of the reaction amplitude derived by Arthurs and Dalgarno[41] for the scattering of a rigid rotor by a structureless atom to relate the complex coefficients of our partial wave expansion to the various scattering matrix elements. While fitting the experimental H-SARP and V-SARP angular distributions, the complex coefficients appearing in Eq. (7) in the partial wave expansion must be related to the same set of scattering matrix elements to ensure that the complex coefficients are internally consistent. As discussed in the supplementary material, we were able to reduce drastically the number of terms in the partial wave expansion because the input and output quantum states in our experiments were highly defined. Table I gives expressions for the complex amplitudes of the outgoing orbitals in terms of the scattering matrix elements, as well as their values determined by fitting our experimental data using Mathematica's NonlinearModelFit function.[42]

We first considered fitting the H-SARP angular distribution because H-SARP prepares HD in a pure state in our chosen coordinate system, and so, the scattering amplitudes can be expressed in terms of a minimum number of partial waves, namely, $Y_{l',0}(\theta, \varphi)$. The contributions of both positive and negative HD–He collision velocities with respect to the +Z axis defined in Figs. 2 and 3 were carefully taken into account in the fitting procedure.

TABLE I. The relative values of the complex amplitudes $c_{l'm_{l'}}$ of the possible outgoing orbital states for H-SARP and V-SARP scattering in Eq. (7) and their expressions in terms of the relevant scattering matrix elements $S^J(jl;j'l')$.

Outgoing partial wave $Y_{l',m'_l}(\theta,\varphi)$	Complex amplitude $c_{l'm_{l'}}$	Outgoing wave amplitude expressed in terms of scattering matrix elements $S^J(jl;j'l')$
Y_{00}	1	$S^{J=0}(22;00)$
Y_{10}	≈0	$\sqrt{6/5}S^{J=1}(21;01)$
Y_{20}	$1.4e^{-(2.7)i}$	$S^{J=2}(20;02) + \sqrt{10/7}S^{J=2}(22;02)$
Y_{30}	≈0	$\sqrt{9/5}S^{J=3}(21;03)$
Y_{40}	$0.6e^{3i}$	$\sqrt{18/7}S^{J=4}(22;04)$
Y_{22}	$0.9e^{-(0.6)i}$	$S^{J=2}(20;02) - \sqrt{10/7}S^{J=2}(22;02)$
Y_{32}	≈0	$S^{J=3}(21;03)$
Y_{42}	$0.4e^{3i}$	$\sqrt{15/14}S^{J=4}(22;04)$

TABLE II. Estimated relative amplitudes and phases of the scattering matrix elements $S^J(jl; j'l')$ determined by fitting the experimentally measured angular distributions of H-SARP (Fig. 2) and V-SARP (Fig. 3) prepared HD ($v = 1$, $j = 2$). $S^J(jl; j'l')$ defines the amplitude of the outgoing spherical wave with orbital angular momentum l' generated by the scattering of the incoming spherical wave l, for a given collision channel with a total angular momentum J. The amplitudes are normalized to the value of $S^{J=2}(22; 00)$, and all phases are defined relative to the phase of $S^{J=2}(22; 00)$, which is arbitrarily set to zero.

		Outgoing partial waves				
		$l' = 0$	$l' = 1$	$l' = 2$	$l' = 3$	$l' = 4$
Incoming partial waves	$l = 0$	...	...	$S^{J=2} = 0.58e^{(4.3)i}$	...	...
	$l = 1$	...	~0	...	~0	...
	$l = 2$	$S^{J=0} = 1$	...	$S^{J=2} = 0.84e^{(3.2)i}$	...	$S^{J=4} = 0.37e^{(3)i}$

A fit of our H-SARP data using Eq. (7) showed that the odd outgoing orbitals do not contribute significantly to our measured angular distribution. When we considered only the even outgoing orbital states, we found that the angular distribution could be fit extremely well ($R^2 = 0.99$). This result led us to conclude that the even outgoing waves completely dominate the scattering process.

Because the complex amplitudes are interrelated by the scattering matrix elements, for our partial wave analysis to be internally consistent, the H-SARP fit must also describe the V-SARP angular distribution because the scattering matrix is independent of the M state. We searched the constrained $c_{l'm_{l'}}$ parameter space in the vicinity of the H-SARP fit to find values that improved the fit to our V-SARP data. This search resulted in the set of complex amplitudes shown in Table I, which simultaneously optimized the fits to both the H-SARP ($R^2 = 0.99$) and V-SARP ($R^2 = 0.97$) angular distributions. A complete description of the fitting procedure is given in the supplementary material. The scattering matrix elements in Table I show that the incoming orbitals l that can generate a given outgoing orbital l' are determined by a $\Delta l = 0, \pm 2$ selection rule, which results from the quadrupolar interactions present in the $\Delta j = 2$ scattering considered here.

As detailed in the supplementary material, our experimental control over the collision process drastically reduced the number of scattering matrix elements involved. The combined simplicity in the internal and external states involved allowed us to extract an internally consistent estimate of the relative phase and amplitude of the scattered orbitals, thus in essence finding an estimate of the scattering matrix elements involved in the HD–He collision considered here, which are shown in Table II. The relative amplitudes of the S-matrix elements clearly show dominance of the $l = 2$ input orbital over the barrierless s-wave ($l = 0$), suggesting the existence of an orbiting resonance. We note here that our measurement only allows the determination of the relative and not the absolute phase of the scattering matrix elements. This is because the inelastically scattered angular distribution, which results from interference of the outgoing scattered orbitals, is sensitive only to their relative phase, and thus, the absolute phase remains undefined. The phase of the complex scattering matrix given in Table II is defined relative to the largest matrix element $S^{J=2}(22; 00)$, the phase of which is arbitrarily set equal to zero.

VALIDATING THE SCATTERING MATRIX ELEMENTS USING X-SARP SCATTERING

Before using the fitted scattering matrix elements in Table II to understand the dynamics of the scattering process, we tested their validity using a third m state. For this purpose, we prepared the m entangled state given in Eq. (3), which does not have any $m = 0$ or $m = \pm 2$ components. Because the scattering matrix is independent of the m state, we are able to calculate the angular distribution resulting from the scattering of HD ($v = 1$, $j = 2$, $m = \pm 1$) using our previously determined values of $S^J(jl; j'l')$. Figure 4 shows that the calculated angular distribution using the scattering matrix elements determined by fitting our H-SARP and V-SARP data compares well with the experimentally measured X-SARP scattering angular distribution. The discrepancy near 90° arises from a small, undetermined angle between the molecular beam axis and the polarization direction of the Stokes laser. We

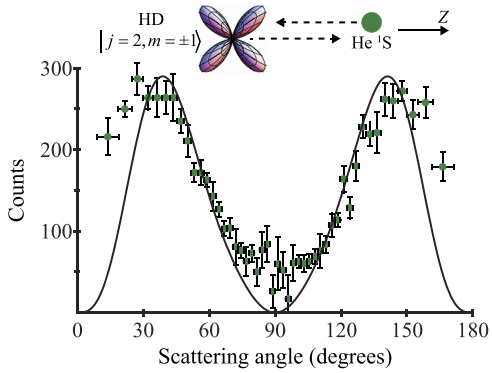

FIG. 4. HD–He X-SARP scattering angular distribution. The green dots give the experimentally measured angular distribution for scattered HD ($v' = 1$, $j' = 0$) molecules generated by rotationally inelastic collisions of the m entangled state HD ($v = 1$, $j = 2$, $m = \pm 1$) defined in Eq. (3) with He. The m quantum number gives the rotational angular momentum component along the Z-axis shown in the inset. After subtracting the off-resonant background, a total of ~8000 scattered molecules were recorded over a period of 288 000 laser pulses. The solid black curve shows the angular distribution calculated using the scattering matrix elements in Table II. The inset describes the input quantum state for this scattering event, wherein the HD bond axis is prepared in a biaxial distribution.

note that for the H-SARP and V-SARP measurements, the SARP laser polarizations were set by minimizing the reflection from a window at Brewster's angle attached to the vacuum chamber, ensuring that the polarizations of both beams were exactly parallel (H-SARP) or perpendicular (V-SARP) to the molecular beam axis. However, because X-SARP uses cross-polarized pump and Stokes laser pulses, it was not possible to verify the laser polarization axis in this way, leading to a nonzero angle between the Stokes polarization and the molecular beam axis. The agreement between the experimentally measured and calculated angular distributions demonstrates that the fit-derived scattering matrix in Table II consistently describes the $\Delta j = 2$ rotationally inelastic scattering of HD by He.

PARTIAL WAVE ANALYSIS ELUCIDATES COLLISION DYNAMICS

Although the collision energy allows scattering for $l = 0$, 1, and 2, the complex amplitudes given in Tables I and II clearly show that the $l = 2$ input state makes the largest contribution to the scattering cross section. Classically, the dominance of the $l = 2$ input orbital is counterintuitive because it faces a higher centrifugal barrier than the barrierless s-wave ($l = 0$) or the p-wave ($l = 1$). However, quantum scatterers have a finite probability of tunneling through this barrier, which is enhanced in the presence of a bound state in the proximity of the collision energy.[43,44] Thus, the dominance of the $l = 2$ input partial wave suggests a possible quasibound HD–He state trapped inside the centrifugal well generated by this angular momentum, resulting in a resonance that mitigates the effects of the centrifugal barrier. Although our collision energy spectrum is wide enough to support resonances for both the $l = 1$ and $l = 2$ input orbital waves, our experimental measurements clearly show that the odd outgoing orbitals $l' = 1$ and 3, which relate to the input $l = 1$ orbital by virtue of the quadrupolar interaction, do not contribute to the measured angular distribution.

Traditionally, scattering resonances are identified by a measured increase in the integral scattering cross section as the center of the narrow input translational energy distribution is tuned.[5,45–48] We instead use partial wave analysis to fit the measured angular distribution collected for a relatively broad range of collision energies, thus determining the relative amplitudes of the outgoing scattered states originating from each incoming partial wave. Unlike the direct measurement available using collision spectroscopy, we infer a resonance from the observed fact that a single input partial wave dominates the measured scattering angular distribution. The dominance of a single partial wave ($l_{res} = 5$ or 6) in the scattering angular distribution at resonance has been previously observed by Vogels *et al.*[5] in the low energy, state selected collisions NO (1/2 f) + He → NO (5/2 f) + He. They have shown that because a single resonant input orbital dominates the scattering, the angular distribution serves as a fingerprint for the resonant state of the collision complex.[5] We note that because of the higher collision energy (13–45 cm^{-1}) present in the NO + He collision experiment, there was a substantial background signal originating from the scattering of the many off-resonant partial waves. By contrast, our low collision energy (0–5 K) limited the number of involved partial waves, reducing the nonresonant background. By measuring the angular distributions resulting from the scattering of several precisely controlled quantum states at these low collision temperatures, our partial wave analysis revealed that the $l = 2$ input orbital dominates the scattering process, thus identifying a possible scattering resonance.

Our partial wave analysis also provided us with insight into the stereodynamics of the collision process. Because it is difficult to compare the number of measured counts in the H-SARP, V-SARP, and X-SARP experiments due to uncertainty in the exact number of molecules prepared in each initial state, we have used Tables I and II to calculate the relative intensities of the HD ($v = 1$, $j = 2$, m) → ($v' = 1$, $j' = 0$) scattering for $m = 0$, ±1, and ±2. Figure 5 compares the calculated angular distributions for these three different initial HD ($v = 1$, $j = 2$, m) states, showing that the scattering of $m = 0$ is four times stronger than that of the $m = \pm 1$ and ±2 initial states. This result makes it apparent that the strong side peaks in the V-SARP angular distribution arise from the dominant $m = 0$ component of the superposition state in Eq. (2). Thus, our determined stereodynamics is consistent with the visual similarity between the V-SARP and H-SARP angular distributions. The dominance of the $m = 0$ state runs counter to our classical intuition that the V-SARP state, where the HD bond axis is perpendicular to the collision velocity, would more efficiently make a rotational transition than H-SARP.

Figure 5 also demonstrates that the observed symmetry in the scattering angular distributions shown in Figs. 2–4 does not result from our experimental geometry but instead is a characteristic of the scattering process. In particular, we note that if the collision velocity distribution is symmetric about zero, it can give rise to a symmetric experimental angular distribution even when the center-of-mass angular distribution is asymmetric. However, in our experiment, the collision velocity distribution is highly asymmetric and therefore cannot be responsible for the observed scattering symmetry (see the supplementary material).

Mathematically, an asymmetric angular distribution results from the interference of odd and even outgoing orbitals. As mentioned above, for the present cold collision involving a low reduced

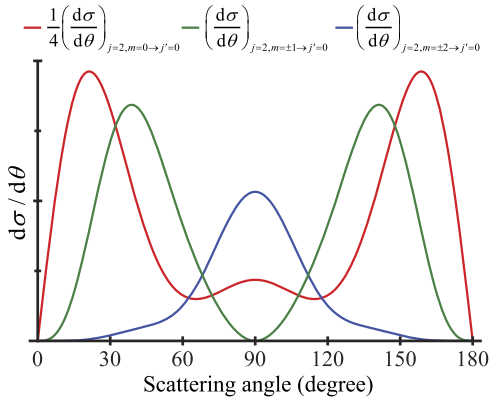

FIG. 5. HD–He stereodynamics. The red, green, and blue curves give the scattering angular distribution $d\sigma/d\theta$ calculated using the scattering amplitudes shown in Tables I and II produced by HD ($v = 1$, $j = 2$, m) → ($v' = 1$, $j' = 0$) scattering for $m = 0$ (red curve), ±1 (green curve), ±2 (blue curve). Note that the angular distribution of HD ($v = 1$, $j = 2$, $m = 0$) is divided by 4, showing that it most efficiently scatters into the final ($v' = 1$, $j' = 0$) state.

mass system, only three input orbitals $l = 0, 1, 2$ contribute to the scattering. For the $\Delta j = 2$ rotational relaxation studied here, the incoming orbitals l that can generate a given outgoing orbital l' are determined by a $\Delta l = 0, \pm 2$ selection rule, and so, an asymmetric angular distribution is possible only if the $l = 1$ and $l = 0$ and 2 input orbitals scatter with comparable cross sections at the same collision energy. Therefore, in the presence of a broad input collision energy distribution, one would expect a large asymmetric background arising from off-resonant scattering of all of the input orbitals. In contrast with the asymmetric distribution observed in an earlier experimental study at higher collision energy,[49] the symmetry of our scattering angular distributions thus provides an additional piece of evidence for the dominance of one of the input orbital states over all the others, implying the existence of a scattering resonance. This implication is reinforced by the abovementioned NO + He study showing that the intensity of the backward scattered peak became comparable to that of the forward scattered peak only when the collision energy was tuned to resonance.[5] Additionally, we note that the off-resonant contribution to this inelastic scattering is expected to be weak. This is because the anisotropic part of the interaction potential that is responsible for the $\Delta j = 2$ transition is a very short range. At a collision energy of a few Kelvin, the input $l = 1$ and 2 orbitals must penetrate the centrifugal barrier to reach the region where the anisotropic forces are large, and therefore, substantial scattering can occur only in the presence of a resonance.

Calculations on HD–He collisions for a variety of rovibrational de-excitation transitions as well as elastic scattering have predicted several resonances in our collision energy region.[32,50–52] However, none of these studies directly addressed the conditions present in our experiment nor did they examine the stereodynamics of the resonant state. The theoretical study most similar to the experiments presented here revealed a resonance near 0.2 cm^{-1} for the HD $(v = 0, j = 2) \rightarrow (v' = 0, j' = 0)$ rotational relaxation.[53] A small fraction of the collisions in our experiment do occur with this energy, but it is not possible to make a direct comparison because scattering resonances can depend sensitively on the vibrational state.[32]

CONCLUSION

Figure 6 graphically describes the quantum state controlled scattering experiment presented in this paper. Our ability to prepare HD in a single rovibrational energy eigenstate with m state precision using SARP and to reduce the collision temperature in the range of a few Kelvin allowed us to extract detailed dynamical information on the He–HD atom-diatom collision, a very simple neutral scattering system, using a partial wave analysis of the scattering angular distribution. The high precision state selection and low collision energy substantially reduced the number of incoming and outgoing orbitals in the partial wave expansion. This simplification in our data analysis allowed us to establish a correlation between the incoming and outgoing orbitals. The correlation determined from fitting the measured angular distributions for two different initial orientations of HD showed that a single incoming partial wave with orbital angular momentum $l = 2$ makes the dominant contribution to the scattering angular distribution. This work thus provides a concrete demonstration of the widely known principle that the amount of information about a collision process that can be extracted from experimental measurement is limited only by the precision with which the input and output quantum states can be defined and measured, respectively.

By determining the probability amplitude of a particular incoming orbital state transforming into its associated outgoing scattered orbitals, we have phenomenologically estimated the scattering matrix elements for the states involved in our collision experiment. To validate our fit-derived scattering amplitudes, we used them to calculate the angular distribution for an entangled m state

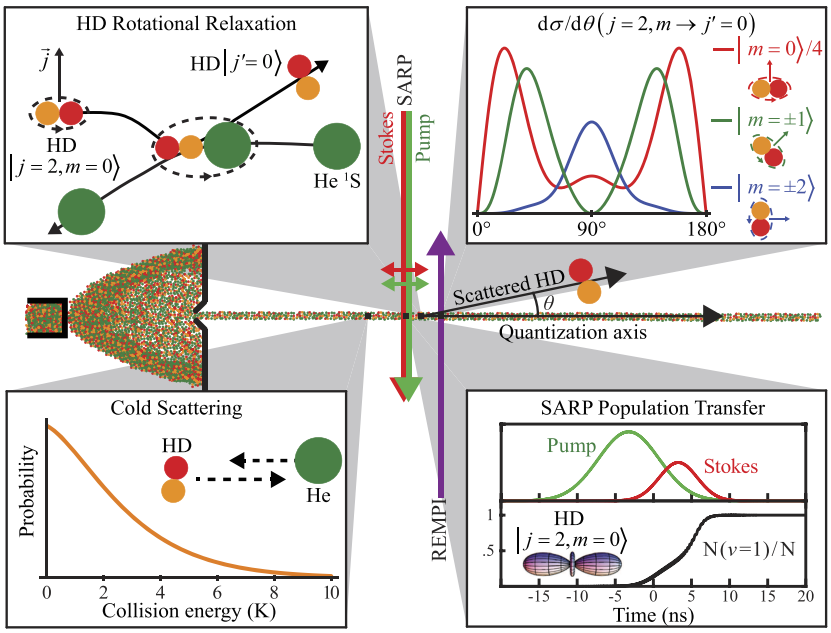

FIG. 6. Graphical representation of quantum state controlled scattering. A coexpanded beam of HD and He is used to generate low energy collisions (bottom left panel). HD molecules are then state-prepared in various orientational (m) sublevels of the HD ($v = 1$, $j = 2$) state using SARP (bottom right panel). For the axis orientation parallel to the relative velocity, the HD–He collision pair transiently forms a quasi-bound complex before the HD is inelastically scattered into the ($v = 1$, $j = 0$) state (top left panel). After state-selectively measuring the angular distribution and fitting using partial wave analysis, we determine that the scattering angular distribution as well as the efficiency depend sensitively on the initial orientation of HD (top right panel).

and showed that our calculation closely matched the experimental result. The partial wave analysis provided us with additional insight into the scattering process by showing a fourfold preference for the input HD $m = 0$ state. To our knowledge, a stereodynamic preference of this magnitude has never before been observed in an inelastic collision. Furthermore, the preference for the $m = 0$ input state, which corresponds to the HD bond axis parallel to the collision velocity, is classically counterintuitive. These experiments thus show that even the simple hydrogen-helium scattering system is ripe for further exploration, both experimentally and theoretically.

SUPPLEMENTARY MATERIAL

The supplementary material contains additional information on the following topics: 1. (4 + 1) REMPI of ground state He atoms. 2. Lab-frame vs center-of-mass frame angular distribution and symmetry. 3. Partial-wave analysis to determine the scattering amplitudes. 4. Selection against odd orbitals. 5. Preparation and scattering of the X-SARP state. 6. Resonant bound state enhances tunneling.

ACKNOWLEDGMENTS

This work has been supported by the U.S. Army Research Office under ARO Grant No. W911NF-16-1-1061.

REFERENCES

[1]D. R. Herschbach, "Reactive scattering in molecular beams," in *Advances in Chemical Physics*, edited by J. Ross (John Wiley & Sons, 1966), Vol. 10, pp. 319–393.
[2]R. D. Levine, *Molecular Reaction Dynamics* (Cambridge University Press, 2005).
[3]R. N. Zare, "Laser control of chemical reactions," Science **279**, 1875–1879 (1998).
[4]R. V. Krems, "Cold controlled chemistry," Phys. Chem. Chem. Phys. **10**, 4079–4092 (2008).
[5]S. N. Vogels *et al*, "Imaging resonances in low-energy NO-He inelastic collisions," Science **350**, 787–790 (2015).
[6]W. E. Perreault, N. Mukherjee, and R. N. Zare, "Quantum control of molecular collisions at 1 Kelvin," Science **358**, 356–359 (2017).
[7]W. E. Perreault, N. Mukherjee, and R. N. Zare, "Quantum controlled rotationally inelastic scattering of HD with H_2 and D_2 near 1 Kelvin reveals collisional partner reorientation," Nat. Chem. **10**, 561–567 (2018).
[8]M. Brouard, D. H. Parker, and S. Y. T. van de Meerakker, "Taming molecular collisions using electric and magnetic fields," Chem. Soc. Rev. **43**, 7279–7294 (2014).
[9]P. Dittmann *et al*, "The effect of vibrational excitation ($3 \leq v' \leq 19$) on the reaction Na_2 (v') + Cl → NaCl + Na^*," J. Chem. Phys. **97**, 9472 (1992).
[10]H. J. Loesch, "Orientation and alignment in reactive beam collisions: Recent progress," Annu. Rev. Phys. Chem. **46**, 555–594 (1995).
[11]M. H. G. de Miranda *et al*, "Controlling the quantum stereodynamics of ultracold bimolecular reactions," Nat. Phys. **7**, 502–507 (2011).
[12]M. Brouard *et al*, "Fully quantum state-resolved inelastic scattering of NO(X) + Kr: Differential cross sections and product rotational alignment," J. Chem. Phys. **141**, 164306 (2014).
[13]C. Naulin and M. Costes, "Experimental search for scattering resonances in near cold molecular collisions," Int. Rev. Phys. Chem. **33**, 427–446 (2014).
[14]J. Jankunas and A. Osterwalder, "Cold and controlled molecular beams: Production and applications," Annu. Rev. Phys. Chem. **66**, 241–262 (2015).
[15]N. Mukherjee, W. E. Perreault, and R. N. Zare, "Stark-induced adiabatic passage processes to selectively prepare vibrationally excited single and superposition of quantum states," in *Frontiers and Advances in Molecular Spectroscopy* (Elsevier, 2018), pp. 1–46.
[16]N. Mukherjee and R. N. Zare, "Stark-induced adiabatic Raman passage for preparing polarized molecules," J. Chem. Phys. **135**, 024201 (2011).
[17]W. Dong, N. Mukherjee, and R. N. Zare, "Optical preparation of H_2 rovibrational levels with almost complete population transfer," J. Chem. Phys. **139**, 074204 (2013).
[18]N. Mukherjee, W. Dong, and R. N. Zare, "Coherent superposition of M-states in a single rovibrational level of H_2 by Stark-induced adiabatic Raman passage," J. Chem. Phys. **140**, 074201 (2014).
[19]W. E. Perreault, N. Mukherjee, and R. N. Zare, "Supersonic beams of mixed gases: A method for studying cold collisions," Chem. Phys. **514**, 150–153 (2018).
[20]C. Amarasinghe and A. G. Suits, "Intrabeam scattering for ultracold collisions," J. Phys. Chem. Lett. **8**, 5153–5159 (2017).
[21]J. Andres *et al*, "The anisotropic interaction potential of D_2Ne from state-to-state differential cross sections for rotational excitation," J. Chem. Phys. **73**, 5620–5630 (1980).
[22]U. Buck, "Rotationally inelastic scattering of hydrogen molecules and the non-spherical interaction," Faraday Discuss. Chem. Soc. **73**, 187–203 (1982).
[23]A. Schiffman and D. W. Chandler, "Experimental measurements of state resolved, rotationally inelastic energy transfer," Int. Rev. Phys. Chem. **14**, 371–420 (1995).
[24]H. Kohguchi, T. Suzuki, and M. H. Alexander, "Fully state-resolved differential cross sections for the inelastic scattering of the open-shell NO molecule by Ar," Science **294**, 832–834 (2001).
[25]K. T. Lorenz *et al*, "Direct measurement of the preferred sense of NO rotation after collision with argon," Science **293**, 2063–2066 (2001).
[26]H. Chadwick *et al*, "Inelastic scattering of NO by Kr: Rotational polarization over a rainbow," J. Phys. Chem. Lett. **5**, 3296–3301 (2014).
[27]M. C. Van Beek, J. J. Ter Meulen, and M. H. Alexander, "Rotationally inelastic collisions of OH($X^2\Pi$) + Ar. II. The effect of molecular orientation," J. Chem. Phys. **113**, 637–646 (2000).
[28]J. J. van Leuken, J. Bulthuis, S. Stolte, and J. G. Snijders, "Steric asymmetry in rotationally inelastic state-resolved NO-Ar collisions," Chem. Phys. Lett. **260**, 595–603 (1996).
[29]B. Nichols *et al*, "Steric effects and quantum interference in the inelastic scattering of NO(X) + Ar," Chem. Sci. **6**, 2202–2210 (2015).
[30]D. R. Flower, "HD in the primordial gas," Mon. Not. R. Astron. Soc. **318**, 875–878 (2000).
[31]D. R. Flower, J. Le Bourlot, G. Pineau Des Forêts, and E. Roueff, "The cooling of astrophysical media by HD," Mon. Not. R. Astron. Soc. **314**, 753–758 (2000).
[32]J. L. Nolte, P. C. Stancil, T. G. Lee, N. Balakrishnan, and R. C. Forrey, "Rovibrational quenching rate coefficients of HD in collisions with He," Astrophys. J. **744**, 62 (2012).
[33]W. Meyer, P. C. Hariharan, and W. Kutzelnigg, "Refined *ab initio* calculation of the potential energy surface of the He–H_2 interaction with special emphasis to the region of the van der Waals minimum," J. Chem. Phys. **73**, 1880 (1980).
[34]N. Balakrishnan, R. C. Forrey, and A. Dalgarno, "Quenching of H_2 vibrations in ultracold ^{3}He and ^{4}He collisions," Phys. Rev. Lett. **80**, 3224–3227 (1998).
[35]R. Forrey, N. Balakrishnan, A. Dalgarno, M. Haggerty, and E. Heller, "Quasiresonant energy transfer in ultracold atom-diatom collisions," Phys. Rev. Lett. **82**, 2657–2660 (1999).
[36]U. Even, "The Even-Lavie valve as a source for high intensity supersonic beam," EPJ Tech. Instrum. **2**, 17 (2015).
[37]W. E. Perreault, N. Mukherjee, and R. N. Zare, "Angular and internal state distributions of H_2^+ generated by (2 + 1) resonance enhanced multiphoton ionization of H_2 using time-of-flight mass spectrometry," J. Chem. Phys. **144**, 214201 (2016).
[38]W. E. Perreault, N. Mukherjee, and R. N. Zare, "Preparation of a selected high vibrational energy level of isolated molecules," J. Chem. Phys. **145**, 154203 (2016).
[39]E. P. Wigner and L. Eisenbud, "Higher angular momenta and long range interaction in resonance reactions," Phys. Rev. **72**, 29–41 (1947).
[40]J. M. Blatt and L. C. Biedenharn, "The angular distribution of scattering and reaction cross sections," Rev. Mod. Phys. **24**, 258–272 (1952).
[41]A. M. Arthurs and A. Dalgarno, "The theory of scattering by a rigid rotator," Proc. R. Soc. London, Ser. A **256**, 540–551 (1960).
[42]Wolfram Research, Inc., Mathematica, 2017.

[43]J. P. Toennies, W. Welz, and G. Wolf, "Molecular beam scattering studies of orbiting resonances and the determination of van der Waals potentials for H–Ne, Ar, Kr, and Xe and for H_2–Ar, Kr, and Xe," J. Chem. Phys. **71**, 614–642 (1979).
[44]A. Klein *et al*, "Directly probing anisotropy in atom–molecule collisions through quantum scattering resonances," Nat. Phys. **13**, 35–38 (2017).
[45]R. Skodje *et al*, "Resonance-mediated chemical reaction: F + HD → HF + D," Phys. Rev. Lett. **85**, 1206–1209 (2000).
[46]A. B. Henson, S. Gersten, Y. Shagam, J. Narevicius, and E. Narevicius, "Observation of resonances in penning ionization reactions at sub-kelvin temperatures in merged beams," Science **338**, 234–239 (2012).
[47]E. Lavert-Ofir *et al*, "Observation of the isotope effect in sub-kelvin reactions," Nat. Chem. **6**, 332–335 (2014).
[48]A. Bergeat, J. Onvlee, C. Naulin, A. Van Der Avoird, and M. Costes, "Quantum dynamical resonances in low-energy CO(j = 0) + He inelastic collisions," Nat. Chem. **7**, 349–353 (2015).
[49]D. W. Martin and P. E. Siska, "Differential nonreactive scattering of He^* (2^1S, 2^3S) by D_2 and H_2: Anisotropic optical potentials and comparison with *ab initio* theory," J. Chem. Phys. **82**, 2630–2643 (1985).
[50]J. Schaefer, "Rotational integral cross sections and rate coefficients of HD scattered by He and H_2," Astron. Astrophys., Suppl. Ser. **85**, 1101–1125 (1990).
[51]E. Roueff and C. J. Zeippen, "Rotational excitation of HD molecules by He atoms," Astron. Astrophys. **343**, 1005–1008 (1999).
[52]J. L. Nolte *et al*, "Isotope effects in complex scattering lengths for He collisions with molecular hydrogen," Phys. Rev. A: At., Mol., Opt. Phys. **81**, 014701 (2010).
[53]B. Zhou and M. Chen, "Quantum rotational scattering of H_2 and its isotopologues with He," Mol. Phys. **115**, 2442–2450 (2017).